A&A 422, 29–38 (2004)
DOI: 10.1051/0004-6361:20030621

Astronomy & Astrophysics

K_s-band luminosity function of the z = 1.237 cluster of galaxies RDCS J1252.9-2927⋆

S. Toft[1,2], V. Mainieri[3], P. Rosati[4], C. Lidman[5], R. Demarco[6], M. Nonino[7], and S. A. Stanford[8,9]

[1] Astronomical Observatory, University of Copenhagen, Juliane Maries Vej 30, 2100 Copenhagen Ø, Denmark
[2] Department of Astronomy, Yale University, PO Box 208101, New Haven, CT 06520-8101, USA
e-mail: toft@astro.yale.edu
[3] Max-Planck-Institut für extraterrestrische Physik, Postfach 1319, 85748 Garching, Germany
[4] European Southern Observatory, Karl-Schwarzchild-Strasse 2, 85748 Garching, Germany
[5] European Southern Observatory, Alonso de Cordova 3107, Casilla 19001, Santiago, Chile
[6] Institut d'Astrophysique de Paris, 98bis Boulevard Arago, 75014 Paris, France
[7] Instituto Nazionale di Astrofisica, Osservatorio Astronomico de Trieste, via G.B. Tiepolo 11, 34131 Trieste, Italy
[8] Department of Physics, University of California at Davis, 1 Shields Avenue, Davis, CA 95616, USA
[9] Institute of Geophysics and Planetary Physics, LLNL, Livermore, CA 94551, USA

Received 3 November 2003 / Accepted 14 April 2004

Abstract. Using deep VLT/ISAAC near-infrared imaging data, we derive the K_s-band luminosity function (LF) of the z = 1.237 massive X-ray luminous cluster of galaxies RDCS J1252.9-2927. Photometric redshifts, derived from deep multi-wavelength $BVRIzJK_s$ data, and calibrated using a large subset of galaxies with spectroscopic redshifts, are used to separate the cluster galaxy population from the foreground and background field galaxy population. This allows for a simultaneous determination of the characteristic magnitude K_s^* and faint end slope α of the LF without having to make an uncertain statistical background subtraction. The derived LF is well represented by the Schechter function with $K_s^* = 18.54^{+0.45}_{-0.55}$ and $\alpha = -0.64^{+0.27}_{-0.25}$. The shape of the bright end of the derived LF is similar to that measured at similar restframe wavelengths (in the z-band) in local clusters, but the characteristic magnitude is brighter by $\Delta M_z^* = -1.40^{+0.49}_{-0.58}$ mag. The derived α is similar to the value derived in the K_s-band in the z = 1 cluster of galaxies MG2016+112 but is shallower (at the 2.2σ level) than the value measured at similar restframe wavelength (in the z-band) in clusters in the local universe. The brightening of the characteristic magnitude and lack of evolution in the shape of the bright end of the LF suggests that the massive cluster ellipticals that dominate the bright end of the LF were already in place at z = 1.237, while the flattening of the faint end slope suggest that clusters at $z \sim 1$ contains relatively smaller fractions of low mass galaxies than clusters in the local universe.
The results presented in this paper are a challenge for semi analytical hierarchical models of galaxy formation which predict the characteristic magnitude to grow fainter and the faint end slope to steepen with redshift as the massive galaxies break up into their progenitors. The observed evolution is consistent with a scenario in which clusters are composed of a population of massive galaxies which formed at high redshift ($z \gg 1$) and subsequently evolved passively, and a population of lower mass galaxies which are gradually accreted from the field, primarily at lower redshift ($z < 1$).

Key words. galaxies: clusters: individual: RDCS J1252.9-2927 – galaxies: elliptical and lenticular, cD – galaxies: evolution – galaxies: formation – galaxies: luminosity function, mass function – cosmology: observations

1. Introduction

The galaxy luminosity function (LF) is a powerful tool for constraining models of galaxy formation and evolution. The LF of both field and cluster galaxies have been shown to be well represented by the Schechter function $\phi(m)\mathrm{d}m = n^* \left[10^{0.4(m^*-m)}\right]^{\alpha+1} \mathrm{e}^{-10^{0.4(m^*-m)}} \mathrm{d}m$, where m^* is the characteristic magnitude of the distribution, α is the faint end slope, and n^* is a normalization constant describing the space density of galaxies.

The variation of the LF parameters with galaxy type (early-type/late-type), wavelength (UV, optical, near-infrared [NIR]) and environment (cluster versus field) and their evolution with redshift depends on the details of mass assembly and star formation and therefore provide strong constraints on galaxy evolution models.

At optical wavelengths the LF of field galaxies and cluster galaxies have been derived from a number of studies (e.g., Garilli et al. 1999; Blanton et al. 2001; Goto et al. 2002;

⋆ Based on observations obtained at the European Southern Observatory using the ESO Very Large Telescope on Cerro Paranal (ESO program 166.A-0101).

Blanton et al. 2003; Christlein & Zabludoff 2003; de Propris et al. 2003). The resulting LF parameters varies somewhat from study to study, most likely due to differences in the data quality and the employed methods for selecting complete samples of galaxies and deriving their luminosity functions.

The most extensive studies are derived from the Sloan Digital Sky Survey (York et al. 2000). Initial results based on the SDSS commissioning data (Blanton et al. 2001; Goto et al. 2002) disagreed with results from the literature, probably due to problems with the photometry, k-corrections and evolutionary corrections. Studies based on more recent data, however, agree better with the literature and do not seem to have such problems (Blanton et al. 2003; Popesso et al. 2004). These studies show that the LF of field galaxies and cluster galaxies are very similar. The LF in both cases has brighter characteristic magnitudes and steeper slopes in the redder bands than in the bluer bands. The faint end slope is slightly steeper for cluster galaxies than for field galaxies in all bands, while the characteristic magnitude from these studies appear to depend very little on environment.

Rich evolved clusters with cD galaxies tend to have flatter faint end slopes than poorer clusters, indicating a deficiency of star forming dwarf galaxies in rich clusters (Lopez-Cruz et al. 1997; Driver & De Propris 2003). Barkhouse et al. (2002) find a tendency for the faint end slope, of the LF of local clusters, to steepen with cluster centric distance, consistent with the hypothesis that a large fraction of dwarf galaxies near cluster centers are being tidally disrupted.

While the variation in the LF parameters at optical wavelengths are sensitive to the star formation properties and morphological mix of the underlying galaxy population, the NIR LF is an excellent probe of the mass function of clusters. The K-band flux of a galaxy is a good tracer of its stellar mass (e.g. Gavazzi et al. 1996), is not very sensitive to star formation and attenuation by dust (compared to the optical band) and the k-corrections are fairly small and relatively independent of galaxy type even at high redshifts (e.g. Mannucci et al. 2001). The evolution of the mass function is directly predicted from galaxy formation and evolution models, making the K-band LF of field and cluster galaxies very useful for fundamental testing of the models.

Locally, the field galaxy K-band LF has been derived using the 2 Micron All Sky Survey (2MASS, Jarrett et al. 2000). Early-type and late-type field galaxies have similarly shaped LF but the early-types are brighter (more massive) and less numerous than the late-types (Kochanek et al. 2001). The evolution of the field galaxy K-band LF has been estimated in three broad redshift bins centered on $z = 0.5$, 1.0 and 1.5 using the K20 survey (Pozzetti et al. 2003). No evolution is found in α to $z = 1.0$, in the highest redshift bin the data are not deep enough to constrain it. The characteristic K-band magnitude of the galaxies in the $z = 1$ bin (which includes galaxies in the redshift range $0.75 < z < 1.3$) is consistent with a mild luminosity evolution in the K-band to $z \sim 1$ of $\Delta M^*_K = -0.54 \pm 0.12$. At $z = 1$, the bright end of the LF is still dominated by ellipticals, and only a small decrease in their space density is observed, indicating that the field ellipticals are largely in place at $z = 1$.

In a deep study of the LF of the Coma cluster, de Propris et al. (1998) find a characteristic magnitude $M^*_K = -24.02$ and a faint end slope of $\alpha = -0.78$. If they restrict the fit to "bright" galaxies ($M < M^* + 3$) they find $\alpha = -0.9$. de Propris et al. (1999) studied 38 clusters in the redshift range $0.1 < z < 0.9$ to look for an evolution in the K-band cluster LF. Their data was not deep enough to constrain the faint end slope, so they fixed it on the Coma cluster value $\alpha = -0.9$, and concentrated on searching for an evolution in the properties of the bright end. Using the same method as de Propris et al. (1999) the sample has subsequently been extended to include a few clusters in the redshift range $z = 1.0-1.2$ (Kodama & Bower 2003; Nakata et al. 2001). The conclusion from these studies is that the shape of the bright end of the K-band LF appears unchanged to $z = 1.2$ and the evolution of the characteristic K-band magnitude with redshift $K^*(z)$ is well described by passively evolving galaxies assembled at $z_f > 2$.

A high formation redshift is also inferred from the evolution of the colour magnitude (CM) relation of cluster early-types to $z \sim 1.3$ (Bower et al. 1992; Aragon-Salamanca et al. 1993; Stanford et al. 1998, 1997; Rosati et al. 1999; van Dokkum et al. 2001; Lidman et al. 2004). The simplest explanation for the evolution of the CM relation is the monolithic collapse models (e.g. Eggen et al. 1962) in which the bulk of stars are formed in a single short duration burst at high redshift and subsequently evolve passively, but it can be equally well explained by semi analytical hierarchical models (e.g. Kauffmann & Charlot 1998) in which the stars are formed in the disks of of late-type progenitors which later merge to form the elliptical galaxies, provided that the merging does not trigger significant star formation.

The K-band LF is predicted to evolve quite differently in the two formation scenarios, due to its close relationship with the evolution of the mass function.

If the galaxies were assembled at high redshift and subsequently evolved passively, as predicted by the monolithic models, we expect the characteristic magnitude to brighten with redshift (as a consequence of the passive evolution of the stars) but the shape of the LF to remain the same. If the galaxies were build up through continuous merging over a broader redshift interval as predicted in hierarchical models, we expect the shape of the LF to change with redshift to reflect the accretion history of the cluster and the merging history of the cluster galaxies. A deficiency of the brightest galaxies should appear as the most massive galaxies break up into their progenitors, resulting in a steepening of the bright end of the LF with redshift. If small structures form first and subsequently merge to form larger structures, the faint end slope should steepen with redshift as galaxies break up into their progenitors. In many hierarchical models however, the cluster population grow by accretion of surrounding structures. The accretion history, and the mass spectrum of the accreted structures could influence the evolution of the LF. The Butcher-Oemler effect (Butcher & Oemler 1978) in intermediate redshift clusters is probably due to star formation in low mass galaxies which have been accreted from the field, induced by interaction with the cluster environment (Butcher & Oemler 1984; Fabricant et al. 1991; Smail et al. 1998; van Dokkum et al. 2000; de Propris et al. 2003).

Such an accretion of primarily low mass galaxies could cause the faint end slope to decline with redshift, as a smaller number of low mass galaxies would have had time to be accreted onto the cluster environment at high redshift.

The apparent passive evolution of the bright end of the cluster LF to $z \sim 1$ is a challenge for hierarchical models which predict that the characteristic mass should be a factor of three smaller at $z \sim 1$ than at present (Kodama & Bower 2003). None of the studies mentioned above have been able to constrain the evolution of α. The first constraints on α at high redshift was derived by Toft et al. (2003) who simultaneously fitted K^* and α in the $z = 1$ cluster MG 2016+112. The derived constraints on α are not strong ($\alpha = -0.60^{+0.39}_{-0.33}$), however it is important to keep it free in the fit since it is coupled to the derived value of K^* and its uncertainties. Furthermore it is noted that since α depends on wavelength, and the K-band corresponds roughly to restframe z-band at $z \sim 1$, the derived value should be compared to the local value measured in the z-band rather than in the K-band when studying evolutionary patterns.

In this paper, we derive firm constraints on K^* and α for the K-band LF of the massive, X-ray luminous cluster of galaxies RDCS J1252.9-2927 (Rosati et al. 2004) at $z = 1.237$. We apply the method of Toft et al. (2003) to high quality multi-wavelength NIR and optical photometric data and extensive spectroscopic follow up observations covering a $4' \times 4'$ field around the cluster.

The outline of this paper is as follows: in Sect. 2 we give a brief introduction to the data and describe how cluster galaxies are separated from the field galaxy population using photometric redshifts, calibrated using the spectroscopic data. In Sect. 3 we derive the LF of the cluster galaxies, in Sect. 4 we compare to results from studies of lower redshift clusters to look for an evolution and compare it to model predictions, and in Sect. 5 we summarize and discuss the results. Throughout the paper we assume a flat cosmology, with $\Omega_m = 0.3$, $\Omega_\Lambda = 0.7$ and $H_0 = 70\,\mathrm{km\,s^{-1}\,Mpc^{-1}}$. Magnitudes are in the Vega system.

2. Building a complete sample of cluster galaxies

The observational basis of this study consist of high quality multi-wavelength NIR and optical photometric data of a $4' \times 4'$ field around RDCS J1252.9-2927, supplemented by spectroscopic follow up observations, all obtained at the ESO Very Large Telescope (with the ISAAC, FORS1 and FORS2 instruments). The central part of the field was imaged for 24 h in each of the NIR wavebands: J_s and K_s, and for approximately 1 h in each of the optical wavebands: B, V, R, I and z. The full data set is described in detail in three companion papers: a paper describing the NIR data (Lidman et al. 2004) a paper describing the optical data (Rosati et al. 2004) and a paper describing the spectroscopic data (Demarco et al. 2004).

To derive the luminosity function of the cluster galaxies in RDCS J1252.9-2927 we need a catalog of cluster galaxies which is complete to a certain magnitude. In Fig. 1 we plot a binned representation of the number of detected objects in the K_s-band as function of magnitude (Lidman et al. 2004). From visual inspection of the turnover magnitude in this figure we estimate that the K_s-band data are complete to $K_s = 22.5$.

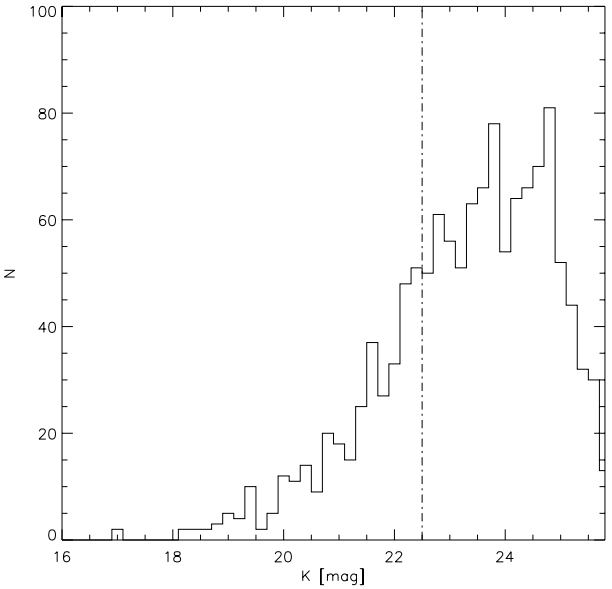

Fig. 1. Binned representation (bin size 0.2 mag) of the number of detected objects as a function of K_s-band magnitude. The data are estimated to be complete to $K_s = 22.5$.

To build a sample of cluster galaxies which is complete to this magnitude, the redshift distribution of all galaxies in the field must be determined in order to separate the cluster galaxy population from the foreground and background populations of galaxies.

At faint magnitudes it is not feasible to obtain this solely through spectroscopic observations. Instead we take advantage of the extensive optical and NIR imaging data to derive photometric redshifts and calibrate and test these against a large subset of galaxies with spectroscopic redshifts.

2.1. Photometry and photometric redshifts

We used SExtractor (Bertin & Arnouts 1996) for object detection in each of the available wave bands, for computing magnitudes in apertures of $2''$ and for cross-correlation of the resulting catalogues. The (3σ) limiting (Vega) magnitudes achieved for the imaging in $2''$ apertures are: $B = 26.7$, $V = 26.8$, $R = 26.0$, $I = 25.7$, $z = 24.3$, $J_s = 23.9$, $K_s = 22.5$.

To obtain reliable colours we must take into account that the imaging in the different wavebands was obtained under different seeing conditions. To derive and apply these corrections we did the following: first, we computed magnitudes in apertures of $2''$ in each of the available ("original") waveband images. We then degraded the point spread function (PSF) of the original images to match the worst seeing condition and recomputed the $2''$ aperture magnitudes in the "degraded" images. The corrections to be applied to the "original" magnitudes was then derived by comparing the magnitudes derived for bright stellar objects in the "original" and the "degraded" images.

We used the Bayesian photometric redshift (BPZ) code of Benítez (2000) to derive photometric redshifts. The advantage of the Bayesian approach is the use of a priori probabilities by which it is possible to include relevant knowledge, such

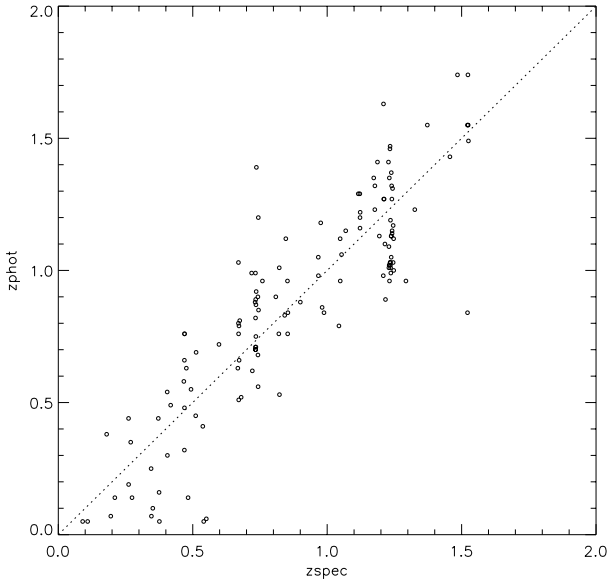

Fig. 2. Photometric redshift ($z_{\rm phot}$) versus spectroscopic redshift ($z_{\rm spec}$) for the full spectroscopic sample. Immediately recognizable is the cluster of galaxies at $z = 1.237$.

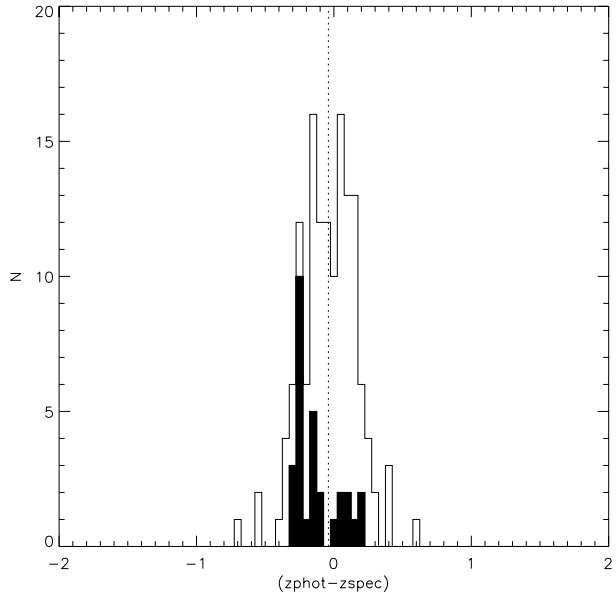

Fig. 3. Distribution of deviations of the photometric redshifts from the spectroscopic redshifts for the spectroscopic cluster member galaxies (filled histogram) and for the full spectroscopic sample (open histogram).

as the expected shape of redshift distributions and the galaxy type fractions, which can be readily obtained from existing surveys. For our study we used the same set of templates as those described in Benítez (2000): four Coleman et al. (1980) templates (E/S0, Sbc, Scd and Irr), and the spectra of two starburst galaxies in Kinney et al. (1996). We derived two interpolated SEDs between each pair of these spectral types. We used the priors derived by Benítez (2000) from the Hubble deep field north (HDFN) and Canada France redshift survey (CFRS) catalogues.

To quantify the reliability of the photometric redshift estimation we used a sample of secure spectroscopic redshifts from our campaign in this area (Demarco et al. 2004). In the region with multi-wavelength coverage described above, there are 120 such spectroscopically identified sources.

In Fig. 2 we plot $z_{\rm phot}$ versus $z_{\rm spec}$ for the spectroscopic sample. The photometric redshifts in general reproduce the spectroscopic redshift well but are systematically smaller. This is illustrated in Fig. 3 where we plot the distribution of deviations of the photometric redshifts from the spectroscopic redshifts. The (sigma clipped) mean of the distribution is $\left\langle z_{\rm phot} - z_{\rm spec} \right\rangle = -0.04$ and the standard deviation is $\sigma = 0.18$. If we restrict the analysis to the spectroscopic cluster members (the filled histogram in Fig. 3) the mean deviation is larger $\left\langle z_{\rm phot} - z_{\rm spec} \right\rangle = -0.13$ and the standard deviation is $\sigma = 0.16$. In Fig. 4 we plot $\left\langle z_{\rm phot} - z_{\rm spec} \right\rangle$ as a function of redshift to investigate whether this is a consequence of a redshift dependent systematic photometric redshift error, which could be introduced by small errors in the photometric zero-points of one or more of the filters. No significant dependency on redshift is observed. In the following we add 0.04 to all the derived redshift to empirically correct for the systematic deviation.

To compare the photometric redshifts errors with those achieved in the literature we define for each object the reduced

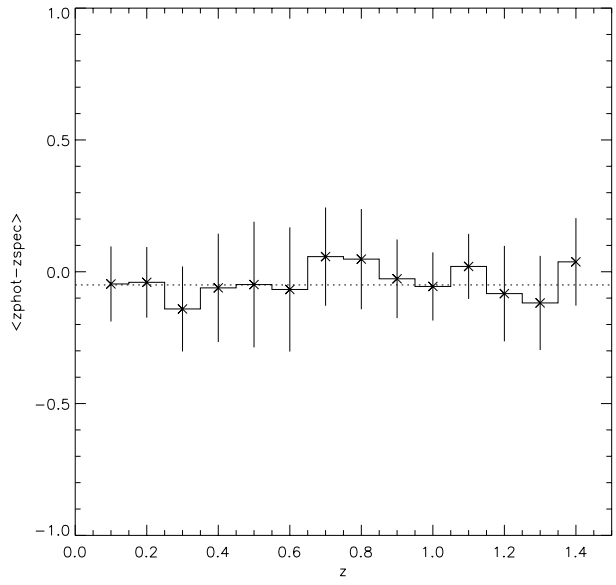

Fig. 4. Mean deviation of the derived photometric redshift from the spectroscopic redshift as a function of spectroscopic redshift, calculated in $\delta = 0.1$ bins. No significant dependency on redshift is observed. The dotted line marks the mean offset −0.04 of the full sample.

error in the photometric redshift estimation as $\delta_z = (z_{\rm phot} - z_{\rm spec})/(1 + z_{\rm spec})$. For the full sample we achieve a mean offset $\langle \delta_z \rangle = 0.02$ and an standard deviation of $\sigma(\delta_z) = 0.11$. If we restrict our analysis to the cluster members we have $\langle \delta_z \rangle = 0.05$ and $\sigma(\delta_z) = 0.09$. The accuracy of our photometric redshifts are comparable to the accuracy achieved by Barger et al. (2003) in a similar Bayesian photometric redshift study of galaxies in the Chandra deep field north. For the HDFN, Benítez (2000) achieve a higher accuracy: $\sigma(\delta_z) = 0.06$, probably due to higher precession Hubble Space Telescope (HST) photometry.

2.2. The photometric cluster member sample

In this section we describe how the cluster galaxy population is separated from the foreground and background field galaxy population using the photometric redshift. We take into account the uncertainty in the photometric redshift estimation by allowing galaxies with photometric redshifts within Δz of the cluster redshift $z_{\rm cl}$ to be classified as "photometric members". The choice of Δz is a trade off between cluster galaxy completeness and field galaxy pollution. The interval must be sufficiently broad to include as many "real" cluster galaxies as possible and sufficiently narrow to minimize pollution from field galaxies. From Figs. 2−4 it can be seen that most cluster member galaxies at $z = 1.237$ are expected to have photometric redshifts in the range $|z_{\rm phot} - z_{\rm cl}| \leq 0.3$. Since we are aiming at building a sample of cluster galaxies which is complete to $K_s = 22.5$ we prioritize not to exclude any cluster members and choose $\Delta z = 0.3$. In the following, galaxies with $0.935 < z_{\rm ph} < 1.535$ are thus classified as photometric members.

To estimate the "completeness function" of the photometric member sample (the fraction of $z = 1.237$ cluster galaxies recovered by the photometric redshift analysis in the Δz interval, as a function of magnitude) we did the following: for each $\delta m = 0.5$ mag bin in the observed range of magnitudes $K_s = 16-23$, we generated a catalog of 1000 galaxies at $z = 1.237$ as they would appear in a dataset with the same band-passes and limiting magnitudes as the data of RDCS J1252.9-2927. The catalog was generated using the *make_catalog* code in the HYPERZ package (Bolzonella et al. 2000) and were drawn randomly from 7 template spectral types (E to Im). We then applied BPZ to the catalogs. In Fig. 5 we plot the fraction of input ($z = 1.237$) galaxies with derived photometric redshifts within $0.935 < z_{\rm ph} < 1.535$ as a function of K_s-band magnitude. Down to a magnitude of $K_s = 21.5$ about 90% of the galaxies are recovered. At $K_s = 22.5$ the recovery rate is 70%. The reason why BPZ appears to be performing slightly worse at the brightest magnitudes, compared to at fainter magnitudes, is that the simulated catalogs contain sizable fractions of bright late-type galaxies which are very rare at $z = 1.237$, and therefore are assigned small probabilities by BPZ, resulting in a some cases, in the most likely spectrum being a lower redshift spectrum of earlier type. The redshift evolution of the field galaxy luminosity function, and its cosmic variance is not known with sufficient accuracy to correctly incorporate the effects of pollution of field galaxies in the completeness function analysis. We return to the issue of field contamination in Sects. 2.3 and 3.

2.3. Spatial distribution of photometric member galaxies

To investigate the spatial distribution of the photometric members galaxies we constructed an image with the pixel value at the centroid of the photometric cluster members equal to one and the remaining pixel values equal to zero. This image was then smoothed with a Gaussian kernel with $FWHM = 60$ pixels (∼8.″8). In Fig. 6 we overlay contours of the smoothed density distribution of the photometric member galaxies on the K_s-band image of the cluster. The contours are 2−10 times the density of galaxies in the HDFN with $K_s < 22.5$ and $0.935 < z_{\rm ph} < 1.535$ (Fernández-Soto et al. 1999).

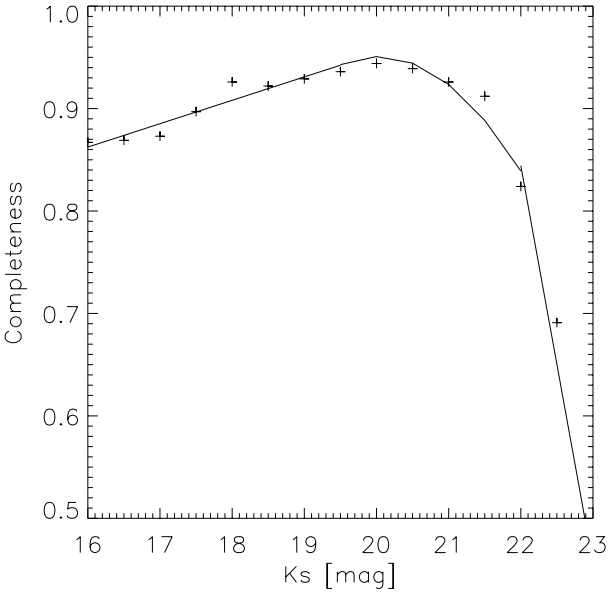

Fig. 5. Completeness function of the photometric member sample, calculated as the fraction of simulated $z = 1.237$ cluster galaxies recovered by the photometric redshift analysis as a function of magnitude.

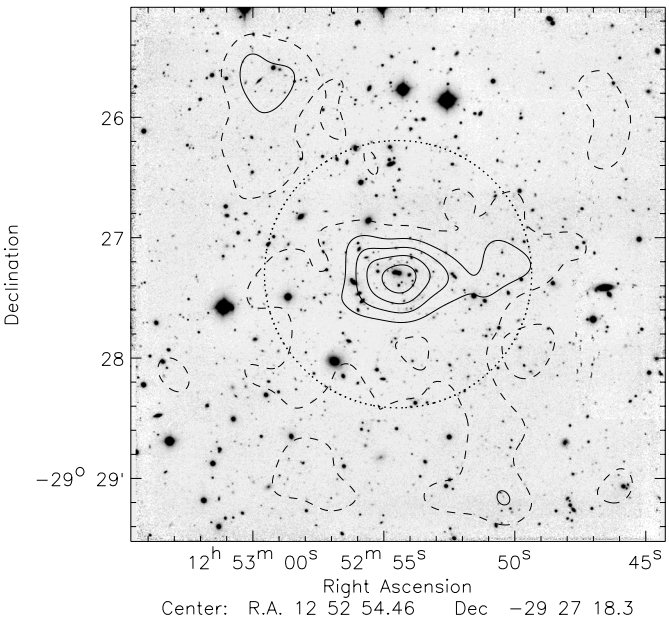

Fig. 6. Contours of the smoothed density distribution of photometric member galaxies overlaid on the ∼4′×4′ mosaic K_s-band ISAAC image (Lidman et al. 2004). The contours are 2 times (dashed line) and 4−10 times (full line) the density of galaxies in the HDFN with $K_s < 22.5$ and $0.935 < z_{\rm ph} < 1.535$ (Fernández-Soto et al. 1999). Inside the dotted circle with radius 65″ the contamination from field galaxies in the photometric member sample is 25%. This circle marks the aperture inside which we derive the cluster galaxy luminosity function of RDCS J1252.9-2927 in Sect. 3.

There is a large concentration of photometric member galaxies in the central part of the field. In this region the

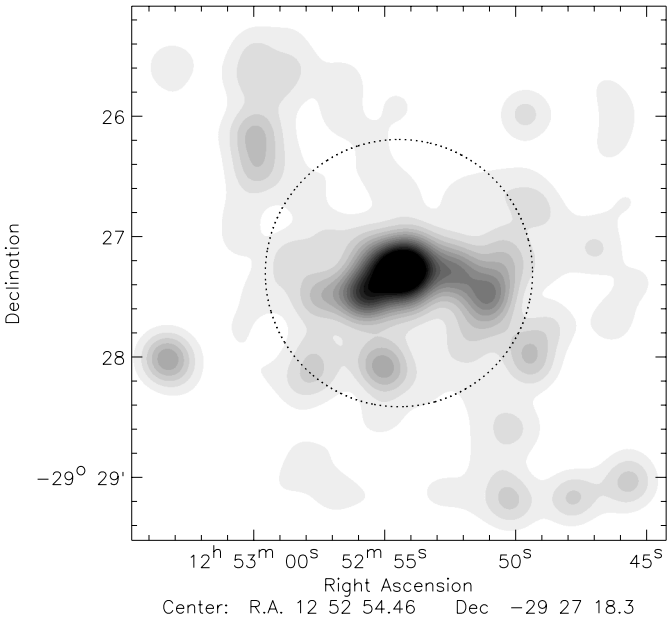

Fig. 7. Map of the smoothed K_s-band light of the photometric member galaxies. The map was generated by creating a version of the K-band image in which pixels inside squares (of size 20 pix × 20 pix) centered on the photometric members were left at their original values and the remaining pixels were set equal to zero. This image was then smoothed with a Gaussian kernel with $FWHM = 60$ pixels. The circle marks the region inside which the LF is derived.

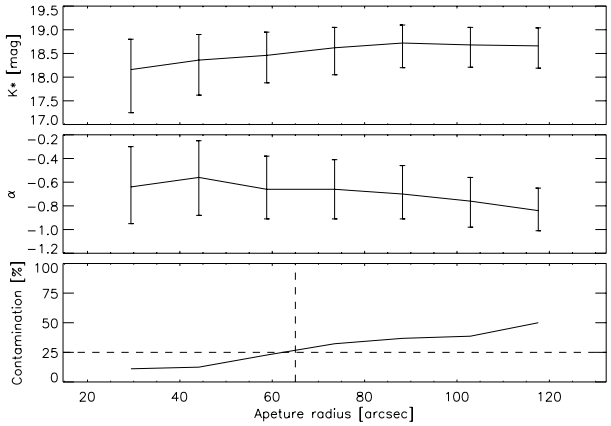

Fig. 8. The top and middle panel shows the K_s^* and α parameters of the LF of the photometric member galaxies derived in apertures of increasing size, centered on the cluster core. Note that the two parameters are not independent, so the error bars in the two plots are correlated. The bottom panel shows the contamination in apertures of increasing size estimated from the subsample of photometric member galaxies with spectroscopic redshifts. The contamination is calculated as the number of interlopers, i.e. photometric member galaxies with spectroscopic redshifts different from the cluster redshift (defined as $1.22 \leq z_{\rm spec} \leq 1.25$), divided by the total number of photometric member galaxies with spectroscopic redshifts. Inside the aperture with radius 65″ (marked by the vertical dashed line), the contamination is 25%.

photometric member sample must thus be dominated by cluster galaxies. The density of photometric members in the outer parts of the field is comparable to the density in the HDFN suggesting that field galaxy pollution could make a significant contribution to the photometric member sample in these regions. We discuss this further in Sect. 3

In addition to the number-density distribution of the photometric member galaxies we also investigated the distribution of their K_s-band light. In Fig. 7 we show a smoothed map of the K_s-band light of the photometric member galaxies. Since the K_s-band flux traces the stellar mass of the cluster galaxies, this map can be be thought of as a stellar mass map of the cluster, which can be compared to maps of the gas mass derived from X-ray observations, and maps of the dark matter derived from weak lensing observations. With this in mind it is interesting to note that, in addition to a strong concentration of light in the center of the cluster, the light is extended in the East-West direction. This extension is also seen seen in both X-ray and weak-lensing mass maps (Lombardi et al. 2004).

3. Luminosity function

We now have a sample of cluster galaxies which is complete to $K_s = 22.5$, or rather a sample which we know how to correct for incompleteness, and we can derive the K_s-band luminosity function of the cluster galaxies without having to make uncertain statistical corrections to account for foreground and background field galaxy contamination. The choice of Δz in Sect. 2.2 ensures that all spectroscopically confirmed cluster members are included in the photometric member sample. To take full advantage of the data we apply the maximum likelihood technique of Schechter & Press (1976) directly to the luminosity distribution of the cluster galaxies rather than doing a "least squares" fit to a binned representation. In this way we include the information that in many magnitude intervals no galaxies are found, and do not make the assumption of the χ^2 method that the underlying distribution is Gaussian. The "incompleteness" of the photometric redshift selection is taken into account through the completeness function shown in Fig. 5. This in turn leads to more realistic error bars. For more details of the method we refer to the appendix of Toft et al. (2003).

In Sect. 2.3 we argued that pollution from field galaxies in the photometric member sample could be significant in the outer parts of the $4' \times 4'$ field. The amount of pollution can be estimated from the subsample of photometric member galaxies with spectroscopic redshifts. These galaxies are likely to constitute a relatively fair sample of galaxies in the relevant redshift range, since the selection of the spectroscopic sample was designed not to introduce biases on the cluster galaxy populations, while minimizing the pollution of field galaxies. This was accomplished by targeting galaxies with $K_s < 21$, $J - K_s < 2.1$ and $R - K_s > 3$. Such criteria do not penalize cluster galaxies, since at $z = 1.237$ even the latest types are redder than $R - K_s = 3$ and early types are bluer than $J - K_s = 2.1$, however field contamination is significantly reduced.

In Fig. 8 the bottom panel shows the contamination derived in apertures with increasing radius (centered on the cluster core). In the central parts of the field the contamination is modest. The pollution within 45″ is ∼10%, within 65″ it is ∼25%, and within 120″ it is 50%. To investigate the effects

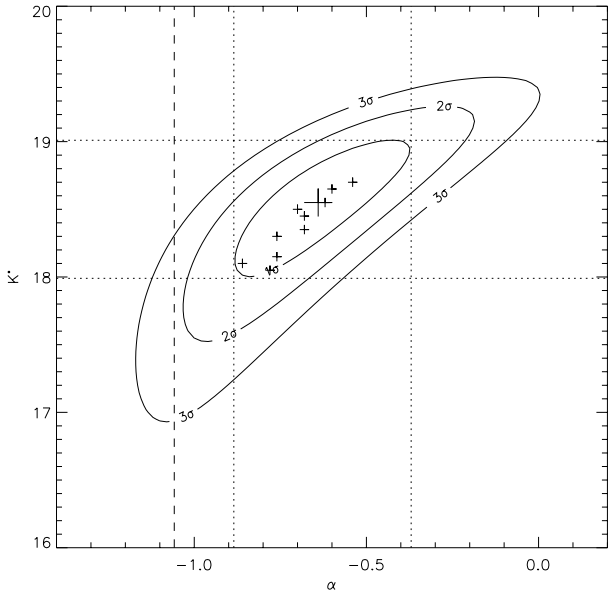

Fig. 9. Contour plot showing the constraints on the Schechter function parameters derived from the maximum likelihood analysis. The big cross marks the best fitting parameters, and the curves represent $1-3\sigma$ confidence levels. The small crosses marks the best fitting parameters for the catalogs with perturbed photometry (see text). The dashed line mark the 1σ upper limit for the faint end slope $\alpha = -1.14 \pm 0.08$ derived in local clusters at similar restframe wavelength (in the z-band, Popesso et al. 2004).

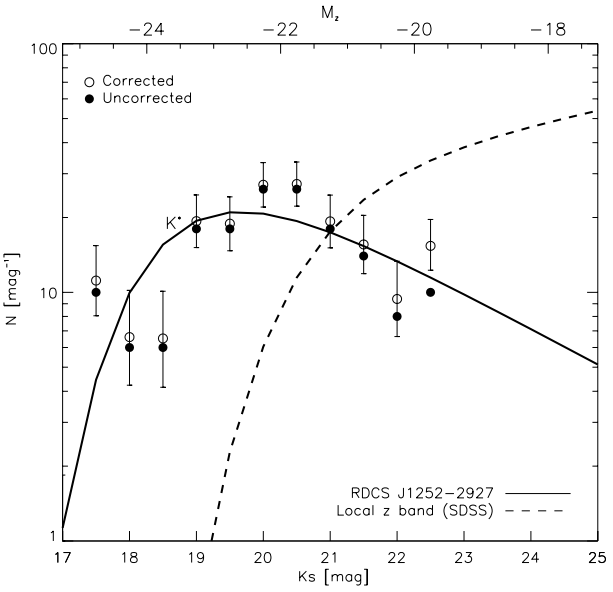

Fig. 10. The full curve is the K_s-band LF of the photometric member galaxies within 65″ of the cluster center, represented by the best fitting Schechter function, with parameters $K_s^* = 18.54^{+0.45}_{-0.43}$ and $\alpha = -0.64^{+0.27}_{-0.25}$. The dashed curve is the local z-band cluster galaxy LF which has $M_z^* = -22.31 \pm 0.20$ and $\alpha = -1.14 \pm 0.08$ (Popesso et al. 2004). The filled symbols are a binned representation of the raw counts, while the open symbols have been corrected for the incompleteness of the photometric redshift selection, using the completeness function in Fig. 5. The conversion between observed K_s-band magnitude and restframe z-band magnitude is given in the text.

of the pollution on our analysis we derived the luminosity function of the photometric member sample in apertures of increasing size. The top and middle panel in Fig. 8 shows the variation of the luminosity function parameters with aperture radius.

There is a tendency for K_s^* to be slightly brighter and α to be slightly smaller (less negative) in apertures encompassing only the central regions where the contamination is small, compared to in larger apertures where the contamination is more pronounced, but the effect is barely significant since the error bars are larger in the smaller apertures due to the smaller number of galaxies. Part of the effect could be caused by intrinsic variation in the properties of the cluster galaxy LF with cluster centric distance, and part of it could be a consequence of field galaxy pollution. Since the effect is not statistically significant however, field galaxy pollution is not likely to significantly affect our results.

Based in Fig. 8 we limit our cluster galaxy LF analysis to galaxies within 65″ of the cluster center, in order to maximize the number of galaxies while minimizing the pollution. The photometric member sample contains 100 galaxies within this distance, including 19 spectroscopically confirmed cluster members and 7 interlopers with spectroscopic redshifts different from $z_{\rm cl}$. We remove the known interlopers from the sample and study the luminosity function of the remaining 93 galaxies in detail in the following.

The Schechter function provides a good fit to the data. In Fig. 9 we plot $1-3\sigma$ likelihood contours of the two Schechter function parameters. There is some degeneracy between the two parameters, but we are able to put firm constraints on both the characteristic magnitude $K_s^* = 18.54^{+0.45}_{-0.55}$ and the faint end slope $\alpha = -0.64^{+0.27}_{-0.25}$. Such accuracy is unprecedented at these redshifts.

Since our analysis is based on photometric redshifts which can be sensitive to photometric errors, the results could potentially be affected by small changes in the photometry. To find out whether this is the case, we carried out a series of Monte Carlo simulations to investigate how sensitive the photometric redshift distribution is to the photometric errors. We generated 10 realizations of the full dataset, by randomly perturbing the photometry of the galaxies within their 1σ error bars. We then derived their photometric redshift distribution, defined a photometric cluster member sample, removed known interlopers and derived their LF in exactly the same way as for the original data set. The best fitting LF parameters of the perturbed datasets (represented by small symbols in Fig. 9) all fall within the 1σ contour of the original dataset, indicating that the LF analysis is robust with respect to photometric perturbations, and that the effect of field galaxies scattering in and out of the Δz interval as the photometry is perturbed is small, otherwise we would expect to see larger variations in the LF parameters.

In Fig. 10 we plot the best fitting Schechter function and a binned representation of the data. For comparison, we plot the local z-band cluster galaxy LF, rather than the local K-band cluster galaxy LF, since the observed K_s-band corresponds roughly to restframe z-band at $z = 1.237$. Following the method of van Dokkum & Franx (1996) absolute z-band

magnitudes M_z can be related to the observed K_s-band magnitudes through:

$$M_{z,AB} = K_{s,AB} - 5 * \log(d_L/10) + 2.5 \log(1+z) + \beta(H-K)_{AB}, \quad (1)$$

where $z = 1.237$ is the redshift, d_L is the luminosity distance in parsec and $\beta(H-K)_{AB}$ is a colour term to compensate for the fact that the redshifted z-band does not match the observed K_s-band exactly. The basic assumption made to derive this expression is that the flux at the redshifted z-band can be related to the observed H and K_s-band flux by $F_\nu(\nu_{z_{\rm band}}(z)) = F_\nu(\nu_H)^\beta F_\nu(\nu_K)^{1-\beta}$. We adopt the value $(H-K)_{AB}(z = 1.25) = 0.57$ predicted by the passive evolution models of Kodama & Arimoto (1997) for an elliptical L^* galaxy formed at $z_f = 3$ (the mean formation redshift of cluster ellipticals derived from their CM relation, Lidman et al. 2004) and calculate $\beta = 0.35$ by assuming a simple power-law for the shape of the SED between ν_H and ν_K.

Contamination from faint field galaxies is not likely to significantly affect the results derived for the cluster galaxy LF in the central part of the field, where the photometric member sample is dominated by bright galaxies, but we note that the main effect of such an contamination would be to overestimate the faint end slope, making the derived faint end slope a formal upper limit to the intrinsic faint end slope of the cluster galaxy LF.

4. LF evolution

The observed K_s-band corresponds roughly to restframe z-band at $z = 1.237$, so the evolution of the z-band LF can be constrained by comparing the observed K_s-band LF with the local z-band cluster LF. This is done in Fig. 10 where we plot the derived K_s-band LF and the z-band LF of clusters in the local universe. For the local LF we adopt the parameters $M_z^* = -22.31 \pm 0.20$ and $\alpha = -1.14 \pm 0.08$ derived by Popesso et al. (2004) for the composite LF of X-ray clusters in the Sloan Digital Sky Survey (SDSS). From Fig. 10 it can be seen that the characteristic magnitude of the restframe z-band LF at $z = 1.237$ is brighter than at $z = 0$. By transforming the observed K_s^* to M_z^* using Eq. (1) an evolution of $\Delta M_z = -1.40^{+0.49}_{-0.58}$ mag is derived for the restframe z-band characteristic magnitude. The observed K_s^* can be converted to absolute (restframe) K_s-band magnitude by applying a k-correction:

$$M_{K_s} = K_s - 5 * \log(d_L/10) - k_{K_s}(z = 1.237). \quad (2)$$

If we adopt $k_{K_s}(z = 1.25) = -0.68$ for the k-correction (Mannucci et al. 2001) and compare to M_K^* derived locally in the Coma cluster, we derive an evolution in the restframe K-band characteristic magnitude of $\Delta M_K = -1.4 \pm 0.6$ mag (assuming that $M_K^* = M_{K_s}^*$), in agreement with the evolution derived in the restframe z-band. The errors quoted for ΔM_z and ΔM_K are dominated by the uncertainty in the derived K_s^*. In Fig. 11 we compare the derived K_s^* with values derived for clusters at lower redshift and the predictions of passive evolution models for the evolution of an L^* galaxy formed at $z_f = 2$, 3 and 5 (Kodama & Arimoto 1997). The observed

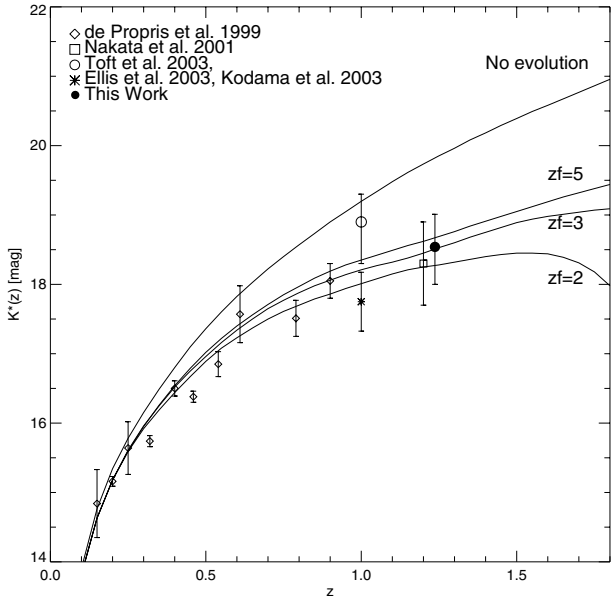

Fig. 11. Evolution of K_s^* with redshift. The curves represent the evolution of an L^* galaxy formed at $z_f = 2$, 3 and 5 predicted by the passive evolution models of Kodama & Arimoto (1997), normalized to the Coma cluster which have $K_s^* = 10.9$ (de Propris et al. 1998). The "no evolution" predictions are calculated using the k-corrections of Mannucci et al. (2001). The data points from the literature have been derived with a fixed $\alpha = -0.9$ (de Propris et al. 1999; Nakata et al. 2001; Ellis & Jones 2004; Kodama & Bower 2003) except for the $z = 1$ value which was was derived with α as a free parameter (Toft et al. 2003). The $z = 1$ data point marked by a star, is the mean K^* of 5 clusters in the redshift range $0.8 < z < 1.1$ (Kodama & Bower 2003; Ellis & Jones 2004), with error bars added in quadrature.

evolution of K^* to $z = 1.237$ is consistent with what is expected for a passively evolving population of galaxies formed at $z_f \gtrsim 2$.

The derived faint end slope $\alpha = -0.64^{+0.27}_{-0.25}$ is similar to the value $\alpha = -0.60^{+0.39}_{-0.33}$ derived in the K_s-band in the $z = 1$ cluster MG 2016+112 (Toft et al. 2003), but shallower (at the 2.2σ level, see Fig. 9) than the value $\alpha = -1.14 \pm 0.08$ derived at similar restframe wavelengths (in the z-band) in local clusters (Popesso et al. 2004), indicating that clusters at $z \sim 1$ contains relatively smaller fractions of low mass galaxies than clusters in the local universe. This is in disagreement with semi analytical hierarchical models which predict the faint end slope to steepen with redshift as the massive cluster galaxies break up into their progenitors.

5. Summary and discussion

In this paper, we have taken advantage of an extensive NIR and optical dataset of the massive, X-ray luminous cluster of galaxies RDCS J1252.9-2927 to derive the first secure constraints on the shape of the K_s-band LF at $z > 1$. The LF was found to be well represented by the Schechter function over the observed range of cluster galaxy magnitudes: $K_s = [17.0{-}22.5]$.

We tested our analysis for the influence of photometric errors and pollution from field galaxies and found our results to be robust and relatively insensitive to the effects of field galaxy

pollution in the central parts of the field where the constraints of the cluster galaxy LF is derived.

The characteristic magnitude $K_s^* = 18.54^{+0.45}_{-0.55}$ is $\Delta M_z = 1.40^{+0.49}_{-0.58}$ mag brighter than the characteristic magnitude measured for clusters in the local universe at similar restframe wavelengths (in the z-band).

This is consistent with studies of the fundamental plane in a cluster at similar redshift where a luminosity evolution of $\Delta M_B = -1.50 \pm 0.13$ was found in the restframe B-band (van Dokkum & Stanford 2003).

Apart from being shifted to systematically brighter magnitudes, the shape of the bright end of the LF at $z = 1.237$ appears similar to in the local universe. Since the K-band LF is a good tracer of the stellar mass function of the cluster galaxies, this suggests that the massive elliptical that dominate the bright end of the LF were already in place at $z = 1.237$. This is a challenge for hierarchical models which predict the bright end of the K-band LF to steepen and K^* to become fainter at high redshift as the massive galaxies break up into their progenitors. At $z \sim 1$, current hierarchical models predict the characteristic mass (closely related to the characteristic K-band magnitude) to be a third of that in the local universe (Kodama & Bower 2003), which is clearly not the case for RDCS J1252.9-2927.

The brightening of the characteristic magnitude, and lack of evolution in the shape of the bright end of the LF to redshift $z = 1.237$ is consistent with a simple formation scenario in which the massive elliptical galaxies that dominate the bright end of the K-band LF are passively evolving systems assembled at high redshift $z_f \simeq 3$.

This formation scenario is also in agreement with the observed properties of the CM-relation of elliptical galaxies in RDCS J1252.9-2927, which is identical to the CM relation found in local clusters in terms of slope and scatter, but bluer on average, consistent with old populations of stars formed at $2.7 < z_f < 3.6$ (Lidman et al. 2004; Blakeslee et al. 2003). From the evolution of the CM relationship alone it is not possible to distinguish between formation scenarios where the old stars are formed in monolithic collapse of the elliptical galaxies at high redshift, and scenarios where they are formed in the disks of less massive late-type galaxies which later merge to form the ellipticals, as long as the merging does not trigger significant star formation. From the lack of evolution in the shape of the bright end of the K-band LF we can however deduce that if the massive ellipticals in clusters formed through merging, it took place at higher redshifts ($z \gg 1$) than is predicted by current semi analytical models.

The results derived here for the evolution of the bright end of the NIR cluster galaxy LF are similar to the results derived from the K20 survey for the evolution of the NIR field galaxy LF (Pozzetti et al. 2003).

The magnitude of the restframe z-band luminosity evolution of cluster galaxies: $\Delta M_z = 1.40^{+0.49}_{-0.58}$ mag to $z = 1.237$, is very similar to what is derived from the K20 survey for $1.0 < z < 1.7$ field galaxies with a similar mean redshift $\langle z \rangle = 1.22$: $\Delta M_z^* = 1.5 \pm 0.5$ mag (Pozzetti, private communication) suggesting that the evolution is not a strong function of environment.

It is interesting to note that a population of massive, evolved and highly clustered galaxies in the redshift range $2 \lesssim z \lesssim 4$ have recently been discovered in deep NIR observations (Franx et al. 2003; van Dokkum et al. 2003; Daddi et al. 2003). These are good candidates for progenitors of the old, massive, passively evolving elliptical galaxies observed in $z \sim 1$ clusters.

The depth of our data allow us to trace the LF down to 4 mag below K_s^*, which is unprecedented at these redshifts, and put firm constraints on the faint end slope of the LF. We derive a slope $\alpha = -0.64^{+0.27}_{-0.25}$ which is similar to the slope measured in the K_s-band in the MG 2016+112 cluster at $z = 1$ but shallower than the value measured at similar restframe wavelengths in clusters in the local universe. The observed evolution in the faint end slope can be interpreted as an evolution in the stellar mass spectrum of the low mass galaxies that dominate the faint end of the K-band LF, indicating that high redshift clusters contains relatively smaller fractions of low mass galaxies than clusters in the local universe. This results is in disagreement with semi analytical hierarchical assembly models, which predict the relative fraction of low mass galaxies to increase, and the faint end slope of the NIR LF to steepen with redshift as massive cluster galaxies break up into lower mass progenitors.

The results presented here are consistent with a scenario in which clusters are composed of a population of massive cluster galaxies which were formed at high redshift ($z \gg 1$) and subsequently evolved passively with little additional star formation and interaction, and a population of lower mass galaxies which are continuously accreted from the field, primarily at lower redshift ($z < 1$).

Acknowledgements. We thank T. Kodama for providing us with his elliptical galaxy evolution models and J. Hjorth for suggestions and discussions which helped improve the analysis and the presentation. We are grateful to the anonymous referee for very helpful comments. This work was supported by the Danish Ground-Based Astronomical Instrument Center (IJAF). Support for SAS came from NASA/LTSA grant NAG5-8430, who is also supported by the Institute of Geophysics and Planetary Physics (operated under the auspices of the US Department of Energy by the University of California Lawrence Livermore National Laboratory under contract W-7405-Eng-48).

References

Aragon-Salamanca, A., Ellis, R. S., Couch, W. J., & Carter, D. 1993, MNRAS, 262, 764
Barger, A. J., Cowie, L. I., Capak, P., et al. 2003, AJ, 126, 632
Barkhouse, W. A., Yee, H. K. C., & López-Cruz, O. 2002, in Tracing Cosmic Evolution with Galaxy Clusters, ASP Conf. Ser., 268, 289
Benítez, N. 2000, ApJ, 536, 571
Bertin, E., & Arnouts, S. 1996, A&AS, 117, 393
Blakeslee, J. P., Franx, M., Postman, M., et al. 2003, ApJ, 596, L143
Blanton, M. R., Dalcanton, J., Eisenstein, D., et al. 2001, AJ, 121, 2358
Blanton, M. R., Hogg, D. W., Bahcall, N. A., et al. 2003, ApJ, 592, 819
Bolzonella, M., Miralles, J.-M., & Pelló, R. 2000, A&A, 363, 476
Bower, R. G., Lucey, J. R., & Ellis, R. S. 1992, MNRAS, 254, 589
Butcher, H., & Oemler, A. 1978, ApJ, 219, 18

Butcher, H., & Oemler, A. 1984, ApJ, 285, 426
Christlein, D., & Zabludoff, A. I. 2003, ApJ, 591, 764
Coleman, G. D., Wu, C.-C., & Weedman, D. W. 1980, ApJS, 43, 393
Daddi, E., Röttgering, H. J. A., Labbé, I., et al. 2003, ApJ, 588, 50
de Propris, R., Eisenhardt, P. R., Stanford, S. A., & Dickinson, M. 1998, ApJ, 503, L45
de Propris, R., Stanford, S. A., Eisenhardt, P. R., & Dickinson, M. 2003, ApJ, 598
de Propris, R., Stanford, S. A., Eisenhardt, P. R., Dickinson, M., & Elston, R. 1999, AJ, 118, 719
Demarco, R., Rosati, P., Mainieri, V., et al. 2004, in prep.
Driver, S.,, & De Propris, R. 2003, Ap&SS, 285, 175
Eggen, O. J., Lynden-Bell, D., & Sandage, A. 1962, ApJ, 136, 748
Ellis, S. C., & Jones, L. R. 2004, MNRAS, 348, 165
Fabricant, D. G., McClintock, J. E., & Bautz, M. W. 1991, ApJ, 381, 33
Fernández-Soto, A., Lanzetta, K. M., & Yahil, A. 1999, ApJ, 513, 34
Franx, M., Labbé, I., Rudnick, G., et al. 2003, ApJ, 587, L79
Garilli, B., Maccagni, D., & Andreon, S. 1999, A&A, 342, 408
Gavazzi, G., Pierini, D., & Boselli, A. 1996, A&A, 312, 397
Goto, T., Okamura, S., McKay, T. A., et al. 2002, PASJ, 54, 515
Jarrett, T. H., Chester, T., Cutri, R., et al. 2000, AJ, 119, 2498
Kauffmann, G., & Charlot, S. 1998, MNRAS, 294, 705
Kinney, A. L., Calzetti, D., Bohlin, R. C., et al. 1996, ApJ, 467, 38
Kochanek, C. S., Pahre, M. A., Falco, E. E., et al. 2001, ApJ, 560, 566
Kodama, T., & Arimoto, N. 1997, A&A, 320, 41
Kodama, T., & Bower, R. 2003, MNRAS, 346, 1
Lidman, C., Rosati, P., Demarco, R., et al. 2004, A&A, 416, 829
Lombardi, M., Rosati, P., Mainieri, V., et al. 2004, in prep.
Lopez-Cruz, O., Yee, H. K., Brown, J. P., Jones, C., & Forman, W. 1997, ApJ, 475, 97
Mannucci, F., Basile, F., Poggianti, B. M., et al. 2001, MNRAS, 326, 745
Nakata, F., Kajisawa, M., Yamada, T., et al. 2001, PASJ, 53, 1139
Popesso, P., Böhringer, H., Brinkmann, J., Voges, W., & York, D. G. 2004, in prep.
Pozzetti, L., Cimatti, A., Zamorani, G., et al. 2003, A&A, 402, 837
Rosati, P., Mainieri, V., Demarco, R., et al. 2004, in prep.
Rosati, P., Stanford, S. A., Eisenhardt, P. R., et al. 1999, AJ, 118, 76
Rosati, P., Tozzi, P., Ettori, S., et al. 2004, AJ, 127, 230
Schechter, P., & Press, W. H. 1976, ApJ, 203, 557
Smail, I., Edge, A. C., Ellis, R. S., & Blandford, R. D. 1998, MNRAS, 293, 124
Stanford, S. A., Eisenhardt, P. R., & Dickinson, M. 1998, ApJ, 492, 461
Stanford, S. A., Elston, R., Eisenhardt, P. R., et al. 1997, AJ, 114, 2232
Toft, S., Soucail, G., & Hjorth, J. 2003, MNRAS, 344, 337
van Dokkum, P. G., Förster Schreiber, N. M., Franx, M., et al. 2003, ApJ, 587, L83
van Dokkum, P. G., & Franx, M. 1996, MNRAS, 281, 985
van Dokkum, P. G., Franx, M., Fabricant, D., Illingworth, G. D., & Kelson, D. D. 2000, ApJ, 541, 95
van Dokkum, P. G., & Stanford, S. A. 2003, ApJ, 585, 78
van Dokkum, P. G., Stanford, S. A., Holden, B. P., et al. 2001, ApJ, 552, 101
York, D. G., Adelman, J., Anderson, J. E., et al. 2000, AJ, 120, 1579